Koo et al. Applied Biological Chemistry (2023) 66:51
https://doi.org/10.1186/s13765-023-00808-z

KSABC
The Korean Society for Applied Biological Chemistry

ARTICLE Open Access

Biochemical characterization of type I-E anti-CRISPR proteins, AcrIE2 and AcrIE4

Jasung Koo[1], Gyujin Lee[1], Donghyun Ka[1], Changkon Park[1], Jeong-Yong Suh[1,2] and Euiyoung Bae[1,2*]

Abstract

In bacteria and archaea, CRISPRs and Cas proteins constitute an adaptive immune system against invading foreign genetic materials, such as bacteriophages and plasmids. To counteract CRISPR-mediated immunity, bacteriophages encode anti-CRISPR (Acr) proteins that neutralize the host CRISPR–Cas systems. Several Acr proteins that act against type I-E CRISPR–Cas systems have been identified. Here, we describe the biochemical characterization of two type I-E Acr proteins, AcrIE2 and AcrIE4. We determined the crystal structure of AcrIE2 using single-wavelength anomalous diffraction and performed a structural comparison with the previously reported AcrIE2 structures solved by different techniques. Binding assays with type I-E Cas proteins were carried out for the target identification of AcrIE2. We also analyzed the interaction between AcrIE4 and its target Cas component using biochemical methods. Our findings corroborate and expand the knowledge on type I-E Acr proteins, illuminating diverse molecular mechanisms of inhibiting CRISPR-mediated prokaryotic anti-phage defense.

Keywords Anti-CRISPR, AcrIE2, AcrIE4, CRISPR–Cas

Introduction

Bacteriophages, also known as phages, are viruses that infect bacteria and archaea [1]. These prokaryotic viruses are ubiquitous with their hosts in the ecosystem [2, 3]. Constant, intense viral infections have led to the development of numerous anti-phage defense systems in bacteria and archaea [4, 5]. One such mechanism is clustered regularly interspaced short palindromic repeat (CRISPR)-mediated prokaryotic immunity against bacteriophages [6, 7]. CRISPRs are a class of repetitive elements found in prokaryotic genomes that consist of invariable 'repeat' sequences interspaced with variable 'spacer' sequences [8–10]. Genes encoding CRISPR-associated (Cas) proteins lie adjacent to the CRISPR arrays [11–13]. CRISPRs and Cas proteins constitute an RNA-based adaptive immune system against invading foreign genetic materials, such as bacteriophages and plasmids [6, 7, 14].

CRISPR-mediated immunity functions through three distinct stages of anti-phage defense [14, 15]. First, Cas proteins form an integrase complex that cleaves and inserts the invading DNA fragments into CRISPR loci as new spacers. Then, the acquired DNA sequences are transcribed as a long precursor CRISPR RNA, which is further processed into mature CRISPR RNAs (crRNAs) containing a single spacer unit. Finally, the crRNAs assemble with Cas protein(s) to form RNA-guided interference complexes for degrading target sequences in re-invading foreign nucleic acids.

CRISPR–Cas systems have been identified in ~40% of bacterial genomes and ~90% of archaeal genomes and can be classified into two major groups and six types [11–13]. In class 1 (types I, III and IV) systems, multiple Cas proteins participate in the formation of the interference complex, whereas class 2 (types II, V and VI) systems use a single multi-domain Cas protein such as Cas9 or Cas12 [11–13, 16]. The type I CRISPR–Cas systems are broadly distributed in various prokaryotic genomes

*Correspondence:
Euiyoung Bae
bae@snu.ac.kr
[1] Department of Agricultural Biotechnology, Seoul National University, Seoul 08826, South Korea
[2] Research Institute of Agriculture and Life Sciences, Seoul National University, Seoul 08826, South Korea

and can be divided into several subtypes depending on their signature Cas components [11, 13]. In type I-E CRISPR–Cas systems, which is one of the most extensively studied subtypes, five Cas proteins (Cas5e, Cas6e, Cas7e, Cas8e, and Cas11) associate with crRNAs to form a CRISPR-associated complex for antiviral defense (Cascade) that recognizes target DNA sequences and directs their degradation by Cas3 nucleases [7, 17].

To counteract CRISPR-mediated immunity, bacteriophages encode anti-CRISPR (Acr) proteins that neutralize the host CRISPR–Cas systems [18]. Several Acr proteins that act against type I-E CRISPR–Cas systems have been found [19–23]. AcrIE2 and AcrIE4 were among those discovered in *Pseudomonas* phages [19]. The structures of AcrIE2 have been determined previously using NMR spectroscopy [24] and X-ray crystallography with ab initio phasing [25]. Co-purification experiments by Mejdani et al. demonstrated that AcrIE2 interacts with Cascade and not with Cas3 [24]. Nevertheless, in their transcriptional reporter assays, the presence of AcrIE2 did not prevent DNA binding of Cascade [24], suggesting a unique inhibition strategy of AcrIE2. To our knowledge, AcrIE4 has not been characterized biochemically. However, it is homologous to the N-terminal domain (NTD) of a fusion Acr protein, AcrIE4-F7, of which we have previously investigated the structure and function [26]. AcrIE4-F7 is encoded by a mobile genetic element in *Pseudomonas citronellolis* [23].

In this study, we describe the biochemical characterization of two type I-E Acr proteins, AcrIE2 and AcrIE4. We determined the crystal structure of AcrIE2 using an experimental phasing technique, and performed in vitro assays to test its binding to individual Cas components comprising the type I-E Cascade. We also analyzed the interaction between AcrIE4 and its target Cas protein using multiple biochemical methods. These results corroborate and expand the knowledge on Acr inhibitors of type I-E CRISPR–Cas systems, highlighting diverse mechanisms for inactivating CRISPR-mediated bacterial anti-phage defense.

Materials and methods

Cloning, expression, and purification of acr proteins

Synthetic AcrIE2 and AcrIE4 genes were cloned into pET21a with a C-terminal $(His)_6$ tag. *Escherichia coli* BL21(DE3) cells transformed with these constructs were cultured in lysogeny broth (LB) medium at 37 °C until the optical density at 600 nm reached 0.6. Protein expression was induced using 1 mM isopropyl β-D-1-thiogalactopyranoside at 17 °C for 16 h. The cells were harvested by centrifugation and resuspended in buffer [500 mM NaCl, 10% (w/v) glycerol, 30 mM imidazole, 5 mM β-mercaptoethanol (BME), 1 mM phenylmethanesulfonyl fluoride, 20 mM 4-(2-hydroxyethyl)-1-piperazineethanesulfonic acid (HEPES) pH 7.0]. After sonication and centrifugation, the resulting supernatant was loaded onto a 5-mL HisTrap HP column (GE Healthcare) pre-equilibrated with buffer [500 mM NaCl, 10% (w/v) glycerol, 30 mM imidazole, 5 mM BME, 20 mM HEPES pH 7.0]. After washing the column, a linear gradient of imidazole (up to 500 mM) was applied to elute the bound proteins. The proteins were further purified by size-exclusion chromatography (SEC) using a HiLoad 16/60 Superdex 75 column (GE Healthcare) equilibrated with buffer [150 mM NaCl, 2 mM 1,4-dithiothreitol (DTT), 20 mM HEPES pH 7.0].

Crystallization and structure determination of AcrIE2

AcrIE2 was crystallized at 20 °C by the sitting-drop vapor diffusion method from 2.3 mM protein solution in buffer [150 mM NaCl, 5% (w/v) glycerol, 2 mM DTT, 20 mM HEPES pH 7.0] mixed with an equal amount of reservoir solution [17% (w/v) polyethylene glycol (PEG) 8000, 200 mM NaCl, 100 mM Na_2HPO_4-citric acid pH 3.8]. To solve the phase problem using single-wavelength anomalous diffraction, selenomethionyl AcrIE2 was expressed in *E. coli* BL21(DE3) cells grown in M9 medium supplemented with selenomethionine, as described previously [27]. The selenomethionyl AcrIE2 protein was purified as described above for native AcrIE2. The selenomethionyl crystals were obtained at 20 °C by the hanging-drop vapor diffusion method from 2.3 mM protein solution in buffer [150 mM NaCl, 5% (w/v) glycerol, 2 mM DTT, 20 mM HEPES pH 7.0] mixed with an equal amount of reservoir solution [17% (w/v) PEG 8000, 200 mM NaCl, 100 mM Na_2HPO_4-citric acid pH 4.2]. The native and selenomethionyl crystals were flash-frozen in liquid nitrogen with additional 12% (w/v) PEG 8000 and 6% (w/v) glycerol as cryoprotecting reagents in the reservoir solution. Diffraction data were collected at beamline 7 A of the Pohang Accelerator Laboratory at 100 K. Diffraction images were processed using HKL2000 [28]. The determinations of selenium positions, density modification, and initial model building for the selenomethionyl AcrIE2 structure were performed using PHENIX [29]. The initial model of the selenomethionyl AcrIE2 was used for phasing the native AcrIE2 structure in PHASER [30]. The final structure was completed using alternate cycles of manual fitting in COOT [31] and refinement in PHENIX [29]. The stereochemical quality of the final model was assessed using MolProbity [32].

Cloning, expression, and purification of Cas proteins

The genes of type I-E Cas proteins were amplified by polymerase chain reaction from the genomic DNAs of *Pseudomonas aeruginosa* PRD-10 and *E. coli* DH5α. They

Table 1 Data collection, phasing, and refinement statistics of AcrIE2

	Native	Selenomethionyl
Space group	$P2_12_12_1$	$P2_12_12_1$
Unit cell parameters (Å)	a = 26.96, b = 47.35, c = 56.37 α = β = γ = 90°	a = 26.95, b = 47.45, c = 56.44 α = β = γ = 90°
Wavelength (Å)	0.9792	0.9792
Data collection statistics		
Resolution range (Å)	50.00–1.23 (1.27–1.23)[a]	50.00–1.44 (1.49–1.44)[a]
Number of reflections	21,354 (2072)[a]	13,392 (1310)[a]
Completeness (%)	98.3 (97.8)[a]	98.4 (97.3)[a]
R_{merge}[b]	0.092 (0.290)[a]	0.123 (2.451)[a]
CC1/2	0.990 (0.974)[a]	0.997 (0.583)[a]
CC*	0.997 (0.993)[a]	0.999 (0.858)[a]
Redundancy	13.8 (13.2)[a]	13.3 (12.2)[a]
Mean I/σ	25.59 (8.84)[a]	11.46 (1.56)[a]
Phasing statistics		
f′, f″ used in phasing		−7.54, 3.36
Figure of merit		0.384
Refinement statistics		
Resolution range (Å)	28.2–1.23	
R_{cryst}[c]/R_{free}[d] (%)	18.1/19.9	
RMSD bonds (Å)	0.006	
RMSD angles (deg)	1.003	
Average B-factor (Å^2)	13.1	
Number of water molecules	118	
Ramachandran favored (%)	100	
Ramachandran allowed (%)	0	

[a] Values in parentheses are for the highest-resolution shell

[b] $R_{merge} = \Sigma_h \Sigma |I_i(h) - < I(h) >| / \Sigma_h \Sigma_i I_i(h)$, where $I_i(h)$ is the intensity of an individual measurement of the reflection and $< I(h) >$ is the mean intensity of the reflection.

[c] $R_{cryst} = \Sigma_h ||F_{obs}| - |F_{calc}|| / \Sigma_h |F_{obs}|$, where F_{obs} and F_{calc} are the observed and calculated structure factor amplitudes, respectively

[d] R_{free} was calculated as R_{cryst} using ~ 5% of the randomly selected unique reflections that were omitted from structure refinement

were cloned into pET28b with an N-terminal $(His)_6$-maltose binding protein (MBP) tag. *E. coli* BL21(DE3) cells containing these constructs were grown in LB medium at 37 °C until the optical density at 600 nm reached 0.6. Expression and purification of the type I-E Cas proteins were performed as described above for the Acr proteins except that a HiLoad 16/60 Superdex 200 column (GE Healthcare) was used during SEC.

Analytical size-exclusion chromatography

Analytical SEC experiments for testing AcrIE2 binding to Cascade subunits were performed using a Superdex 200 10/300 GL column (GE Healthcare) equilibrated with buffer [150 mM NaCl, 2 mM DTT, 20 mM tris(hydroxymethyl)aminomethane-HCl pH 7.5]. Proteins (20 μM each) were mixed in the buffer and incubated at 4 °C for 1 h. The samples (700 μL) were then loaded onto the column at a flow rate of 0.5 mL/min. SEC runs for individual proteins were also performed as control experiments in the same manner. Elution fractions were analyzed by sodium dodecyl sulfate–polyacrylamide gel electrophoresis (SDS-PAGE) and visualized by Coomassie staining. Uncropped gel images are shown in Additional file 1: Figure S1. Analytical SEC runs for testing the interactions between AcrIE4 and Cas8e subunits were performed as described above for AcrIE2 except for using different buffer [150 mM NaCl, 5% (w/v) glycerol, 2 mM DTT, 20 mM HEPES pH 7.0].

Isothermal titration calorimetry (ITC)

ITC was performed at 25 °C using the MicroCal iTC200 calorimeter (Malvern). The $(His)_6$-MBP-tagged Cas8e of

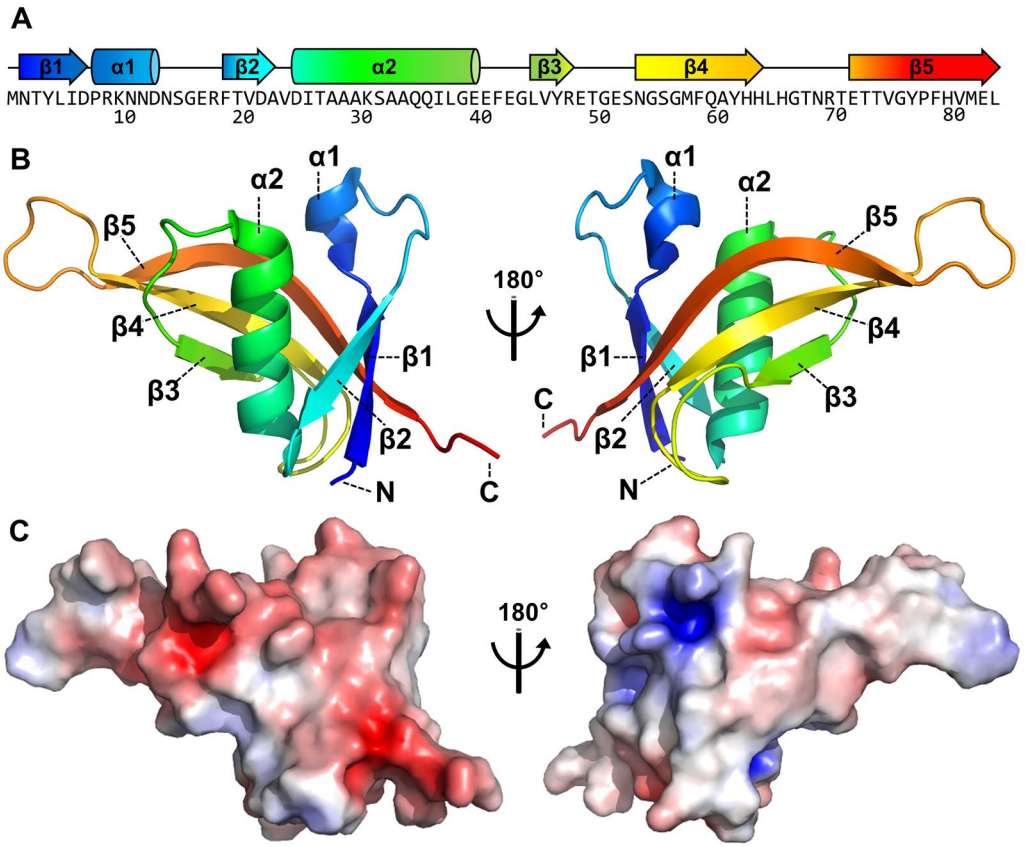

Fig. 1 Structure of AcrIE2. **A** Schematic representation of secondary structures in AcrIE2. Its amino acid sequence is shown and numbered below. **B** Crystal structure of AcrIE2 solved by single-wavelength anomalous diffraction. The structure is shown in rainbow format from the N-terminus (blue) to the C-terminus (red). N- and C-termini and secondary structures are also indicated. **C** Electrostatic potential surface (red = −5.0 kT, blue = +5.0 kT) of AcrIE2 in the same orientation as shown in **B**. The structures were displayed using the PyMOL software (The PyMOL Molecular Graphics System, Version 2.0 Schrödinger, LLC)

P. aeruginosa (20 μM) in a 200-μL sample cell was titrated with 19 consecutive 2-μL injections of AcrIE4 (150 μM) in buffer [150 mM NaCl, 5% (w/v) glycerol, 1 mM tris(2-carboxyethyl) phosphine, 20 mM HEPES pH 7.0]. Origin software (OriginLab) was used to process and analyze the ITC titration data. The integrated heats were least-squared best-fit using a simple one-site binding model, and the errors were obtained from the fitting.

Results and discussion

Crystal structure of AcrIE2

The crystal structure of AcrIE2 was determined to a resolution of 1.35 Å using single-wavelength anomalous diffraction of the selenomethionyl protein. Table 1 summarizes the data collection, phasing, and refinement statistics. AcrIE2 was crystallized in space group $P2_12_12_1$ with a single polypeptide chain and 118 water molecules per asymmetric unit. Residues in the C-terminal $(His)_6$ tag were not modeled in the final structure due to insufficient electron density.

Our crystal structure of AcrIE2 contains two α helices (α1 and α2) and five β strands (β1 to β5) comprising a single antiparallel β sheet (Fig. 1). The shorter α1 helix (residues 8–13) is located in the segment connecting the β1 and β2 strands. The longer α2 helix (residues 25–39) is positioned on the concave side of the five-stranded antiparallel β sheet, contacting residues in all five β strands. Topology and fold of our structure are essentially identical to those of the two previously determined structures (Fig. 2A) [24, 25]. The root mean square deviation (RMSD) values of the 80 Cα atomic positions among the three AcrIE2 structures ranged from 0.4 to 3.0 Å. Our structure is superposed better with the previous crystal structure solved by ab initio phasing than the NMR structure, despite the differences in crystallization

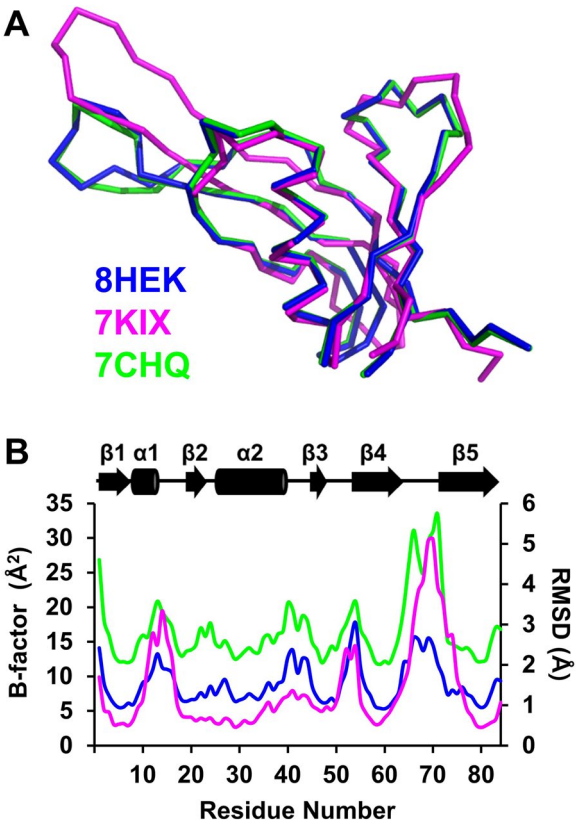

Fig. 2 Comparison of AcrIE2 structures determined by different techniques. **A** Cα-trace superposition of three AcrIE2 structures. Our crystal structure (PDB ID: 8HEK) is superimposed with one of the low-energy structures determined by NMR (PDB ID: 7KIX) and the previous crystal structure solved by ab initio phasing (PDB ID: 7CHQ). The three structures align well except for the loop connecting β4 and β5. Orientation of the superimposed structures is approximately identical to that shown in Fig. 1B. **B** Residual flexibility analyses of AcrIE2 structures. Average crystallographic B-factors of main chain atoms and average RMSD values of Cα atoms from NMR structure ensembles are shown as a function of residue number. Secondary structures of our AcrIE2 structure are also indicated

condition and phasing method. The RMSD between the two crystal structures was only 0.4 Å for 80 Cα atoms.

Despite the high overall structural similarity, local conformational differences were noted between the structures. The most significant discrepancy was observed in the loop connecting the β4 and β5 strands (residues 65–71) (Fig. 2A). The two crystal structures had relatively high crystallographic B-factor values for this segment (Fig. 2B). Residues in the loop region also had relatively high average RMSD values of NMR structure ensembles (Fig. 2B). These observations indicate the highly dynamic nature of this region in the AcrIE2 structures. Thus, the detected structural heterogeneity most likely results from local intrinsic flexibility, which is revealed as different conformations in distinct environments, such as in crystal lattice and bulk solution. The conformational heterogeneity between the two crystal structures is also likely caused by different intermolecular contacts in the crystal lattice. They belong to the same space group ($P2_12_12_1$), and the unit cell parameters (a = 26.96 Å, b = 47.44 Å, c = 56.11 Å, α = β = γ = 90°) of the crystal structure solved by ab initio phasing are very similar to those of our structure (Table 1). However, surface residues involved in crystal contacts are not identical between the two crystal structures (Additional file 1: Table S1). Protein interfaces between AcrIE2 molecules in crystal lattice are also different (Additional file 1: Table S2). Overall, our crystal structure of AcrIE2 contains features similar to those of the two previously reported structures, with minor local conformational heterogeneity despite the technical differences in structure determination.

Test of AcrIE2 binding to Cas components in the type I-E Cascade

Contrary to the type I-F system, the recombinant type I-E Cascade of *P. aeruginosa* is difficult to prepare due to its poor expression and solubility [24, 33]. To identify Cas protein(s) that can bind to AcrIE2 in vivo, Mejdani et al. expressed $(His)_6$-tagged AcrIE2 in *P. aeruginosa* and used Ni-affinity chromatography to detect co-purifying proteins [24]. In this experiment, Cas7e was among the most confidently detected proteins, and other type I-E Cascade subunits were also observed with lower confidence, indicating that AcrIE2 interacts with the Cascade mainly via its Cas7e subunit [24]. To confirm this finding in vitro, we tested whether AcrIE2 interacts with separately purified *P. aeruginosa* Cascade components in analytical SEC. Due to the poor solubility of the individual *P. aeruginosa* Cascade subunits [24, 33], we used N-terminal $(His)_6$-MBP tags to stabilize them in our experimental setting.

In type I-E CRISPR–Cas systems, five Cas species assemble to form the Cascade with a stoichiometry of $Cas8e_1$:$Cas11_2$:$Cas7e_6$:$Cas5e_1$:$Cas6e_1$ (Fig. 3A and B) [15, 16]. Thus, we performed multiple SEC runs, in which AcrIE2 and each of the five $(His)_6$-MBP-tagged Cascade subunits (Cas8e, Cas11, Cas7e, Cas5e, and Cas6e) were incubated together and injected into the column. Unexpectedly, AcrIE2 did not interact with any of the *P. aeruginosa* Cascade subunits in our SEC experiments, as the elution volumes of AcrIE2 were identical regardless of whether the Cascade components were incubated together or not (Fig. 3C). This was surprising since AcrIE2 interacted with the Cascade in the previous study by Mejdani et al. [24]. Moreover, our approach using $(His)_6$-MBP-tagged Cascade subunits was successful for

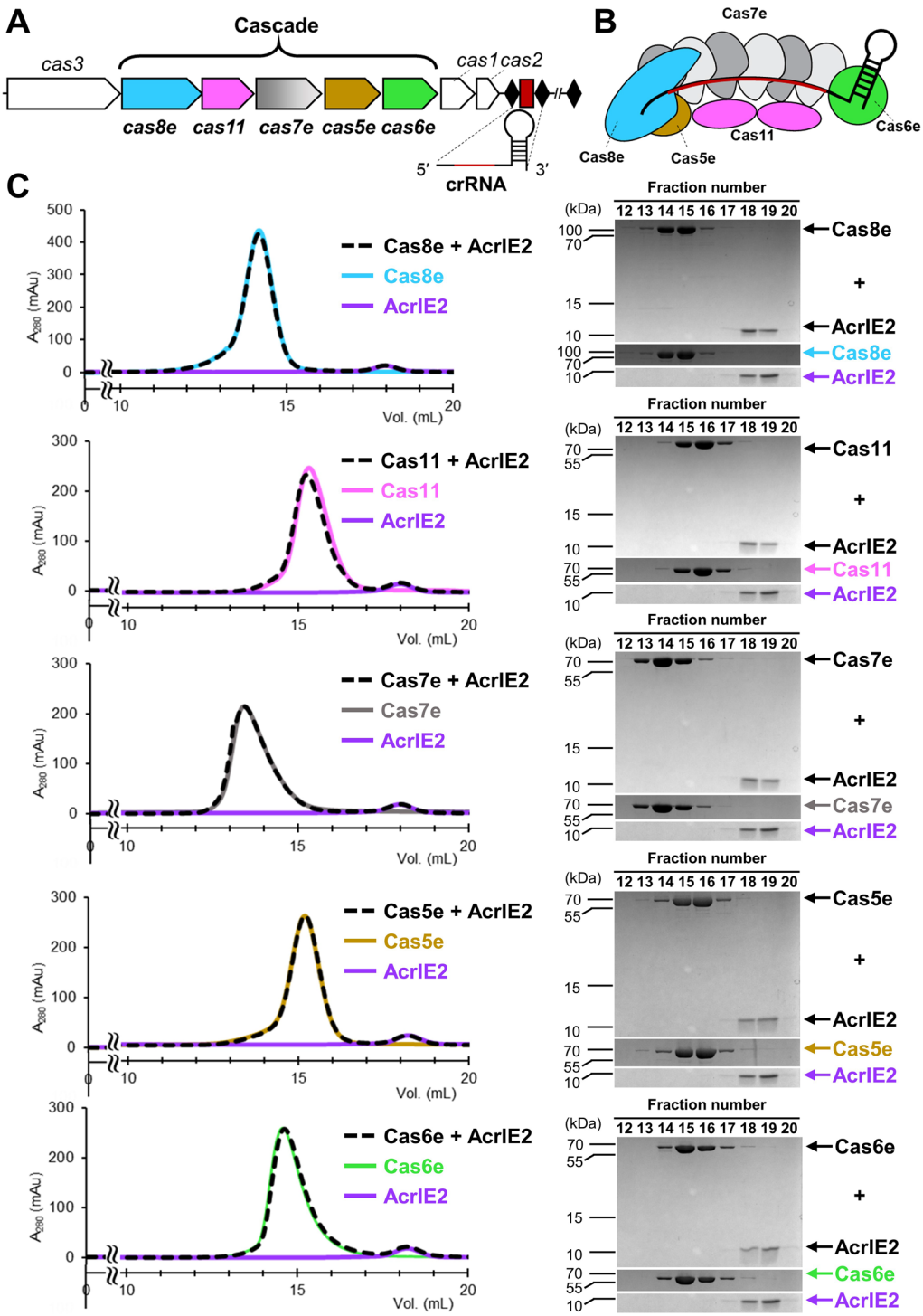

Fig. 3 Test of the interaction between AcrIE2 and type I-E Cascade subunits. **A** Schematic representation of a type I-E CRISPR–Cas locus. Black diamonds and a red rectangle indicate invariable repeats and a variable phage-derived spacer, respectively. **B** Architecture of the type I-E Cascade. The complex has a subunit stoichiometry of $Cas8e_1$:$Cas11_2$:$Cas7e_6$:$Cas5e_1$:$Cas6e_1$:$crRNA_1$. **C** Analytical SEC to evaluate interactions between AcrIE2 and individual Cas components of *P. aeruginosa* type I-E Cascade. AcrIE2 did not co-elute with any of the $(His)_6$-MBP-tagged Cascade subunits. The elution fractions were analyzed by SDS-PAGE. The chromatogram and gel image for AcrIE2 alone are shown repeatedly with those for the five Cascade subunits as a control for comparison. Uncropped gel images are shown in Additional file 1: Figure S1

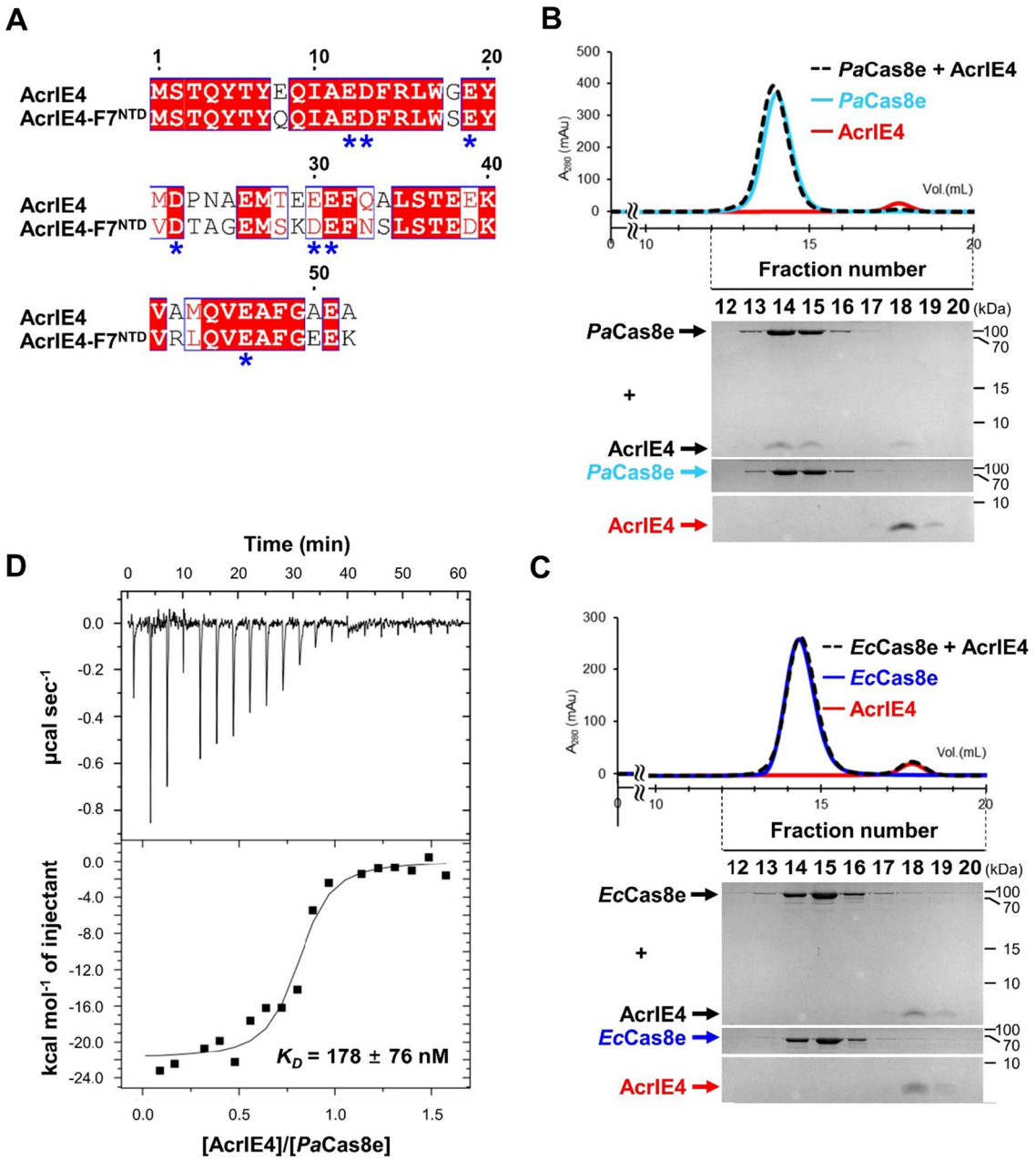

Fig. 4 AcrIE4 targets Cas8e in the type I-E CRISPR–Cas system. **A** Sequence alignment of AcrIE4 and AcrIE4-F7^{NTD}. Conserved negatively charged residues, which were important for the interaction between AcrIE4-F7^{NTD} and Cas8e in our previous study [26], are indicated with blue asterisks. **B**, **C** Analytical SEC experiments for interactions between AcrIE4 and Cas8e homologues. AcrIE4 co-eluted with *P. aeruginosa* Cas8e (**B**), but not with *E. coli* Cas8e (**C**). The elution fractions were analyzed by SDS-PAGE. Uncropped gel images are shown in Additional file 1: Figure S1. **D** ITC analysis of AcrIE4 binding to $(His)_6$-MBP-tagged Cas8e of *P. aeruginosa*. The experimentally determined K_D value is indicated with the fitting errors. *Pa* and *Ec* indicate *P. aeruginosa* and *E. coli*, respectively

target identification of other type I-E Acr inhibitors, such as AcrIE4-F7 [26] and AcrIE4 (see below).

Nonetheless, we suspect that our inability to identify a target Cascade component of AcrIE2 may be due to several potential limitations of our experimental design. First, the N-terminal solubility-enhancing tag may hinder the interaction with AcrIE2. The $(His)_6$-MBP-tag, which is ~42 kDa, could be large enough to occlude a potential binding interface if it is adjacent to the N-terminus. Second, Acr binding to Cascade may require multiple

subunits. Mejdani et al. suggested that AcrIE2 may have more than one functionally important surface [24]. This suggests that AcrIE2 simultaneously interacts with multiple Cascade subunits located in proximity. Last, the solubility-enhancing effect of the $(His)_6$-MBP tag may not be strong enough to fold all of the tested individual Cascade components correctly. We previously identified Cas8e as a single target Cascade subunit for AcrIE4-F7 using the same experimental strategy [26], implying the proper folding of the $(His)_6$-MBP-tagged Cas8e. However, the solubility-enhancing effect of the $(His)_6$-MBP tag may not be guaranteed for other Cascade subunits, such as Cas7e. In the co-purification analyses by Mejdani et al., AcrIE2 interacted mainly with Cas7e [24]. Thus, the more precise Cascade binding mechanism and key interacting Cas residues for AcrIE2 inhibition remain to be determined.

AcrIE4 interacts with *P. aeruginosa* Cas8e

AcrIE4 was discovered in *Pseudomonas* phage D3112 [19]. It contains only 52 amino acid residues and is the smallest (6.0 kDa) among the known type I Acr inhibitors [34]. The fusion Acr inhibitor, AcrIE4-F7, was identified in the mobile genetic element in *P. citronellolis* [23], and the NTD of AcrIE4-F7 (AcrIE4-$F7^{NTD}$) shares high sequence similarity (~69%) with AcrIE4 (Fig. 4A). This fusion Acr protein has been investigated structurally and functionally [26]. However, to our knowledge, biochemical characterization of the original AcrIE4 has not been reported. To this end, we purified recombinant AcrIE4 protein and performed binding assays with a potential Cas target component. Since we previously identified Cas8e as the binding partner for AcrIE4-$F7^{NTD}$ [26], we tested the interaction between AcrIE4 and Cas8e. Due to the poor solubility of *P. aeruginosa* Cas8e [24], we used the N-terminal $(His)_6$-MBP-tagged version for our experiments.

In our analytical SEC experiments (Fig. 4B), AcrIE4 co-eluted with the $(His)_6$-MBP-tagged Cas8e of *P. aeruginosa* when incubated together before injection. The elution volume of the complex was significantly smaller than that of AcrIE4 alone, indicating that AcrIE4 interacted with *P. aeruginosa* Cas8e. In the quantitative analysis using ITC (Fig. 4D), AcrIE4 bound tightly to $(His)_6$-MBP-tagged Cas8e of *P. aeruginosa* with submicromolar affinity. The equilibrium dissociation constant (K_D) was calculated to be ~178 nM, which is comparable with the K_D of ~140 nM determined for AcrIE4-$F7^{NTD}$ in our previous study [26]. Together, these results demonstrate that AcrIE4 binds to the Cas8e subunit of the *P. aeruginosa* type I-E Cascade.

We expect that the binding mode of AcrIE4 to the Cas8e subunit is similar to that of AcrIE4-$F7^{NTD}$. In our additional SEC analyses (Fig. 4C), AcrIE4 did not interact with *E. coli* Cas8e, as observed previously for AcrIE4-$F7^{NTD}$ [26]. The divergence between *P. aeruginosa* and *E. coli* Cas8e proteins has been discussed previously [19, 26], and the preferential Acr binding to the *P. aeruginosa* homologue was attributed to the difference in the protospacer adjacent motif (PAM) recognition site of Cas8e [26]. The PAM interaction surface in *P. aeruginosa* Cas8e includes several non-conserved positively charged residues [26]. The negatively charged (pI ~ 4.2) AcrIE4-$F7^{NTD}$ supposedly acts as a target DNA mimic, interacting with the positively charged PAM-binding residues in *P. aeruginosa* Cas8e [26]. AcrIE4 also has a low pI value (~3.7), and the negatively charged key interacting residues of AcrIE4-$F7^{NTD}$, including Glu19 and Asp22 [26], are also conserved in AcrIE4 (Fig. 4A). Thus, AcrIE4 also likely targets the PAM recognition site in Cas8e in a similar manner to AcrIE4-$F7^{NTD}$.

Supplementary Information

The online version contains supplementary material available at https://doi.org/10.1186/s13765-023-00808-z.

Additional file 1: Table S1. Residues involved in intermolecular contacts (< 4 Å) with symmetry-related neighboring molecules in the crystal lattice. Different residues are indicated in bold. **Table S2.** Protein interface areas with symmetry-related neighboring molecules in crystal lattice. Interface areas were calculated by using PISA (www.ebi.ac.uk/pdbe/pisa). **Figure S1.** Uncropped gel images.

Acknowledgements

We thank the staff of the beamline 7 A of the Pohang Accelerator Laboratory for their support with the data collection, and Suji Hong and Chaewon Jeong for assistance with the cloning.

Author contributions

JK, GL, JS, and EB conceived and designed the study. JK and GL performed the protein purification and analytical SEC. JK, DK, and EB determined the crystal structure. JK, JS, and EB performed the structural analysis. GL, SH, JS, and EB performed the ITC analysis. JK and EB wrote the manuscript with input from all authors.

Funding

This work was supported by the National Research Foundation of Korea grants funded by the Korea government (MSIT) (NRF-2022R1A2C1009804 and RS-2023-00207820) and the Cooperative Research Program for Agricultural Science & Technology Development funded by the Rural Development Administration (PJ01653401).

Availability of data and materials

The atomic coordinates and structure factors were deposited in the Protein Data Bank with the accession code 8HEK.

Declarations

Competing interests

The authors declare no competing financial interests.

Received: 27 May 2023 Accepted: 31 July 2023
Published online: 23 August 2023

References

1. Ofir G, Sorek R (2018) Contemporary phage biology: from classic models to new insights. Cell 172:1260–1270
2. Chevallereau A, Pons BJ, van Houte S, Westra ER (2022) Interactions between bacterial and phage communities in natural environments. Nat Rev Microbiol 20:49–62
3. Weinbauer MG (2004) Ecology of prokaryotic viruses. FEMS Microbiol Rev 28:127–181
4. Hampton HG, Watson BNJ, Fineran PC (2020) The arms race between bacteria and their phage foes. Nature 577:327–336
5. Tesson F, Herve A, Mordret E, Touchon M, d'Humieres C, Cury J, Bernheim A (2022) Systematic and quantitative view of the antiviral arsenal of prokaryotes. Nat Commun 13:2561
6. Barrangou R, Fremaux C, Deveau H, Richards M, Boyaval P, Moineau S, Romero DA, Horvath P (2007) CRISPR provides acquired resistance against viruses in prokaryotes. Science 315:1709–1712
7. Brouns SJ, Jore MM, Lundgren M, Westra ER, Slijkhuis RJ, Snijders AP, Dickman MJ, Makarova KS, Koonin EV, van der Oost J (2008) Small CRISPR RNAs guide antiviral defense in prokaryotes. Science 321:960–964
8. Bolotin A, Quinquis B, Sorokin A, Ehrlich SD (2005) Clustered regularly interspaced short palindrome repeats (CRISPRs) have spacers of extrachromosomal origin. Microbiology 151:2551–2561
9. Mojica FJ, Diez-Villasenor C, Garcia-Martinez J, Soria E (2005) Intervening sequences of regularly spaced prokaryotic repeats derive from foreign genetic elements. J Mol Evol 60:174–182
10. Pourcel C, Salvignol G, Vergnaud G (2005) CRISPR elements in *Yersinia pestis* acquire new repeats by preferential uptake of bacteriophage DNA, and provide additional tools for evolutionary studies. Microbiology 151:653–663
11. Koonin EV, Makarova KS, Zhang F (2017) Diversity, classification and evolution of CRISPR–Cas systems. Curr Opin Microbiol 37:67–78
12. Makarova KS, Wolf YI, Iranzo J, Shmakov SA, Alkhnbashi OS, Brouns SJJ, Charpentier E, Cheng D, Haft DH, Horvath P, Moineau S, Mojica FJM, Scott D, Shah SA, Siksnys V, Terns MP, Venclovas C, White MF, Yakunin AF, Yan W, Zhang F, Garrett RA, Backofen R, van der Oost J, Barrangou R, Koonin EV (2020) Evolutionary classification of CRISPR–Cas systems: a burst of class 2 and derived variants. Nat Rev Microbiol 18:67–83
13. Makarova KS, Wolf YI, Koonin EV (2018) Classification and nomenclature of CRISPR–Cas systems: where from Here? CRISPR J 1:325–336
14. Marraffini LA (2015) CRISPR–Cas immunity in prokaryotes. Nature 526:55–61
15. van der Oost J, Westra ER, Jackson RN, Wiedenheft B (2014) Unravelling the structural and mechanistic basis of CRISPR–Cas systems. Nat Rev Microbiol 12:479–492
16. Nishimasu H, Nureki O (2017) Structures and mechanisms of CRISPR RNA-guided effector nucleases. Curr Opin Struct Biol 43:68–78
17. Xue C, Sashital DG (2019) Mechanisms of type I-E and I-F CRISPR–Cas systems in Enterobacteriaceae. EcoSal Plus 8:ESP-0008
18. Davidson AR, Lu WT, Stanley SY, Wang J, Mejdani M, Trost CN, Hicks BT, Lee J, Sontheimer EJ (2020) Anti-CRISPRs: protein inhibitors of CRISPR–Cas Systems. Annu Rev Biochem 89:309–332
19. Pawluk A, Bondy-Denomy J, Cheung VH, Maxwell KL, Davidson AR (2014) A new group of phage anti-CRISPR genes inhibits the type I-E CRISPR–Cas system of *Pseudomonas aeruginosa*. mBio 5:e00896–e00814
20. Pinilla-Redondo R, Shehreen S, Marino ND, Fagerlund RD, Brown CM, Sorensen SJ, Fineran PC, Bondy-Denomy J (2020) Discovery of multiple anti-CRISPRs highlights anti-defense gene clustering in mobile genetic elements. Nat Commun 11:5652
21. Leon LM, Park AE, Borges AL, Zhang JY, Bondy-Denomy J (2021) Mobile element warfare via CRISPR and anti-CRISPR in *Pseudomonas aeruginosa*. Nucleic Acids Res 49:2114–2125
22. Wang C, Sun Z, Hu Y, Li D, Guo Q, Wang M (2023) A novel Anti-CRISPR AcrIE9.2 is Associated with dissemination of bla(KPC) plasmids in *Klebsiella pneumoniae* sequence type 15. Antimicrob Agents Chemother 67:e01547–e01522
23. Marino ND, Zhang JY, Borges AL, Sousa AA, Leon LM, Rauch BJ, Walton RT, Berry JD, Joung JK, Kleinstiver BP, Bondy-Denomy J (2018) Discovery of widespread type I and type V CRISPR–Cas inhibitors. Science 362:240–242
24. Mejdani M, Pawluk A, Maxwell KL, Davidson AR (2021) Anti-CRISPR AcrIE2 binds the type I-E CRISPR–Cas Complex but does not block DNA binding. J Mol Biol 433:166759
25. Lee SY, Kim GE, Kim YG, Park HH (2020) A 1.3 a high-resolution crystal structure of an anti-CRISPR protein, AcrI E2. Biochem Biophys Res Commun 533:751–757
26. Hong SH, Lee G, Park C, Koo J, Kim EH, Bae E, Suh JY (2022) The structure of AcrIE4-F7 reveals a common strategy for dual CRISPR inhibition by targeting PAM recognition sites. Nucleic Acids Res 50:2363–2376
27. Mark BL, Vocadlo DJ, Knapp S, Triggs-Raine BL, Withers SG, James MN (2001) Crystallographic evidence for substrate-assisted catalysis in a bacterial beta-hexosaminidase. J Biol Chem 276:10330–10337
28. Otwinowski Z, Minor W (1997) Processing of X-ray diffraction data collected in oscillation mode. Methods Enzymol 276:307–326
29. Adams PD, Afonine PV, Bunkoczi G, Chen VB, Davis IW, Echols N, Headd JJ, Hung LW, Kapral GJ, Grosse-Kunstleve RW, McCoy AJ, Moriarty NW, Oeffner R, Read RJ, Richardson DC, Richardson JS, Terwilliger TC, Zwart PH (2010) PHENIX: a comprehensive Python-based system for macromolecular structure solution. Acta Crystallogr D Biol Crystallogr 66:213–221
30. McCoy AJ, Grosse-Kunstleve RW, Adams PD, Winn MD, Storoni LC, Read RJ (2007) Phaser crystallographic software. J Appl Crystallogr 40:658–674
31. Emsley P, Cowtan K (2004) Coot: model-building tools for molecular graphics. Acta Crystallogr D Biol Crystallogr 60:2126–2132
32. Chen VB, Arendall WB III, Headd JJ, Keedy DA, Immormino RM, Kapral GJ, Murray LW, Richardson JS, Richardson DC (2010) MolProbity: all-atom structure validation for macromolecular crystallography. Acta Crystallogr D Biol Crystallogr 66:12–21
33. Pawluk A, Shah M, Mejdani M, Calmettes C, Moraes TF, Davidson AR, Maxwell KL (2017) Disabling a type I-E CRISPR-Cas nuclease with a bacteriophage-encoded Anti-CRISPR protein. mBio 8:e01751–e01717
34. Yin P, Zhang Y, Yang L, Feng Y (2023) Non-canonical inhibition strategies and structural basis of anti-CRISPR proteins targeting type I CRISPR–Cas systems. J Mol Biol 435:167996

Publisher's Note